END

MICROCOPY RESOLUTION TEST CHART
NATIONAL BUREAU OF STANDARDS 1963-A

HIGH PRESSURE STUDIES USING ENERGY DISPERSIVE
DIFFRACTION OF HIGH ENERGY X-RAYS

Final Technical Report

by

W.F. Sherman and D. Häusermann

February 1987

EUROPEAN RESEARCH OFFICE

UNITED STATES ARMY

LONDON, ENGLAND

Wheatstone Laboratory, Department of Physics,

King's College, Strand,

London WC2R 2LS, England.

REPORT DOCUMENTATION PAGE

Form Approved
OMB No 0704 0188
Exp Date Jun 30, 1986

1a. REPORT SECURITY CLASSIFICATION	1b. RESTRICTIVE MARKINGS
Unclassified	None

2a. SECURITY CLASSIFICATION AUTHORITY	3. DISTRIBUTION/AVAILABILITY OF REPORT
	Approved for public release;
2b. DECLASSIFICATION/DOWNGRADING SCHEDULE	distribution unlimited

4. PERFORMING ORGANIZATION REPORT NUMBER(S)	5. MONITORING ORGANIZATION REPORT NUMBER(S)
	R&D 4174-PH-01

6a. NAME OF PERFORMING ORGANIZATION	6b. OFFICE SYMBOL (If applicable)	7a. NAME OF MONITORING ORGANIZATION
King's College London		USARDSG(UK)

6c. ADDRESS (City, State, and ZIP Code)	7b. ADDRESS (City, State, and ZIP Code)
Strand London WC2R 2LS	Box 65 FPO NY 09510-1500

8a. NAME OF FUNDING/SPONSORING ORGANIZATION	8b. OFFICE SYMBOL (If applicable)	9. PROCUREMENT INSTRUMENT IDENTIFICATION NUMBER
AMTL		DAJA45-83-C-0031

8c. ADDRESS (City, State, and ZIP Code)
Watertown
Massachusetts 02172-0001

10. SOURCE OF FUNDING NUMBERS

PROGRAM ELEMENT NO.	PROJECT NO.	TASK NO.	WORK UNIT ACCESSION NO
61102A	1L161102BH57	07	

11. TITLE (Include Security Classification)

(U) High Pressure Studies Using Energy Dispersive Diffraction of High Energy X-Rays

12. PERSONAL AUTHOR(S)
W. F. Sherman and D. Häusermann

13a. TYPE OF REPORT	13b. TIME COVERED	14. DATE OF REPORT (Year, Month, Day)	15. PAGE COUNT
Final	FROM Aug.84 TO Feb.87	1987, March, 3rd	40 + Appendix (176)

16. SUPPLEMENTARY NOTATION

17. COSATI CODES			18. SUBJECT TERMS (Continue on reverse if necessary and identify by block number)
FIELD	GROUP	SUB-GROUP	Energy dispersive diffraction, High energy X-rays,
20	11		Synchrotron radiation, Wiggler, High pressure,
11	06		Drickamer-type cell, TiB, TiB₂.

19. ABSTRACT (Continue on reverse if necessary and identify by block number)

The smooth continuum of white radiation produced by a 160 kV generator has been combined with Energy Dispersive X-Ray Diffraction (EDXRD) and a Drickamer-type cell for high pressure studies. The theory of EDXRD is briefly reviewed and the advantages of the technique, high penetration and improved resolution, are discussed. The results of measurements of the compressibility of TiB up to 80 kbar are reported.

The technique developed has also been used with the high energy radiation produced by the UK Synchrotron Radiation Source Wiggler. A simple diffractometer, designed and built for energy dispersive diffraction of such radiation is described. Results of measurements of the compressibility of TiB2 up to 130 kbar are presented.

20. DISTRIBUTION/AVAILABILITY OF ABSTRACT	21 ABSTRACT SECURITY CLASSIFICATION
☒ UNCLASSIFIED/UNLIMITED ☒ SAME AS RPT. ☒ DTIC USERS	Unclassified

22a. NAME OF RESPONSIBLE INDIVIDUAL	22b TELEPHONE (Include Area Code)	22c OFFICE SYMBOL
Dr. Julian J. Wu	01-409 4423	AMXSN-UK-RP

DD FORM 1473, 84 MAR

83 APR edition may be used until exhausted
All other editions are obsolete.

SUMMARY

The smooth continuum of white radiation produced by a 160 kV generator has been combined with Energy Dispersive X-Ray Diffraction (EDXRD) and a Drickamer-type cell for high pressure studies. The theory of EDXRD is briefly reviewed and the advantages of the technique. high penetration and improved resolution. are discussed. The results of measurements of the compressibility of TiB up to 80 kbar are reported.

The technique developed has also been used with the high energy radiation produced by the UK Synchrotron Radiation Source *Wiggler*. A simple diffractometer. designed and built for energy dispersive diffraction of such radiation is described. Results of measurements of the compressibility of TiB_2 up to 130 kbar are presented.

KEYWORDS

Energy dispersive diffraction. high energy X-rays. synchrotron radiation. wiggler. high pressure, Drickamer-type cell, TiB, TiB_2.

As agreed with Dr. J.J. Wu, this report is based on Chapters 2,3 and 4 of a Doctoral Thesis (Daniel Häusermann, Ph.D., University of London, 1987). The reader who requires a more detailed account of the techniques developed and used for the work reported here should therefore consult the latter, two copies of which are enclosed with the present report. This thesis also includes an extensive liste of references.

CONTENTS

LIST OF FIGURES

LIST OF TABLES

1 - Introduction

In Energy Dispersive X-ray Diffraction (EDXRD) the energy distribution of the photons diffracted at a fixed scattering angle 2θ by a sample placed in a collimated polychromatic beam of X-rays is analysed by an energy sensitive semiconductor detector.

The use of high energy radiation improves both the resolution achievable with the technique and its sensitivity to changes in lattice parameters. It also enables measurements to be made on thick samples and when a high penetration is required.

In the work reported here, we have combined EDXRD, high energy X-rays and a Drickamer-type high pressure cell to measure the equations of state of TiB and TiB_2. The cell was specially designed and built for X-ray diffraction experiments with large samples and within the range of 0 to 200 *kbar*. It uses two opposed tungsten carbide anvils enclosed in steel supports. This design only allows very small windows for the X-ray beams and therefore prevents the use of angular scanning techniques. EDXRD, which uses a fixed geometry, is thus ideally suited to that type of cell. The second feature of such a cell is that the sample is surrounded by several millimetres of packing material which have to be traversed by the X-ray beams. The use of high energy X-rays is therefore essential.

A high voltage generator was used for the measurements of the compressibility of TiB, whilst the radiation produced by the *WIGGLER* of the U.K. Synchrotron Radiation Source (SRS) was used for the other measurements.

2 - The Theory of EDXRD

The basic equation of EDXRD is

$$Ed\sin\theta = constant. \tag{1}$$

where E is the energy of the X-rays, d the separation of the atomic planes within the sample and θ the Bragg angle. If E is expressed in keV and d in $Å$, the *constant* has the value of 6.19926.

With a white (polychromatic) beam of X-rays incident on a powder sample, expression (1) shows that for a fixed value of 2θ discreet values of d will produce reflections in an energy spectrum collected by an energy sensitive detector. This is the principle of EDXRD.

When there are no sample effects causing broadening, the profile of a reflection is the convolution of the profiles of the detector response and that due to the geometry of the collimation system. If both profiles are Gaussian, as in the work reported here, the total Full Width at Half Maximum (FWHM) of a reflection ΔE_T is given by

$$\Delta E_T = \left[k_1 + k_2 E + k_3 E^2\right]^{1/2}, \tag{2}$$

where

$$k_1 = \Delta E_{amp}^2 \text{ and } k_2 = 5.546 F \epsilon \tag{3}$$

are the detector constants and

$$k_3 = (\cot \theta \Delta \theta)^2 \tag{4}$$

the geometrical constant. ΔE_{amp} is the contribution caused by electronic and leakage noises in the preamplifier and the detector respectively, ϵ is the average energy required for creating an electron-hole pair in the semiconductor crystal of the detector (2.96 eV for germanium), F the Fano factor, reflecting the statistical nature of the processes by which a photon deposits its energy E within the crystal, and $\Delta \theta$ the divergence of the collimation system.

3 - Main Features and Advantages of Using High Energy X-Rays

The high voltage generator acquired for this work is manufactured in the U.K. by Pantak Ltd. It has an X-ray tube which can be run up to 160 kV with a maximum electron power loading of 750 W on an effective source size of 0.4 mm x 0.4 mm. Although it is manufactured exclusively for radiographic work, its high brightness makes it a useful tool for diffraction experiments. With a molybdenum target (K_α and K_β lines at 17.4 and 19.6 keV respectively), it produces an extremely smooth spectrum with a useful range of X-ray energies of 20 to 140 kV when operated at 150 kV With a tungsten target, the inconvenience of having the characteristic K_α and K_β lines at approximately 60 keV is minimal and can even be an asset in some cases as we sha.l see later in Section 4.3.

The main advantages of this new source, which produces a smooth spectrum of highly penetrating radiation over a wide energy range, are given below in the context of EDXRD.

3.1 - A Large Dynamic Range

One of the most important parameters in EDXRD is the dynamic range $E_R/\Delta E_D$, which is the range of photon energies in the spectrum , E_R, divided by the energy resolution of the detector ΔE_D. This ratio essentially determines the theoretical maximum number of reflections which can be resolved, and hence its importance. For the detectors used in this work ΔE_D was approximately 320 eV at 25 keV and 460 eV at 75 keV . thus giving dynamic ranges of approximately 150 for a 50 kV generator compared with 300 for the generator used here.

3.2 - High Penetration

The $1/e$ penetration depth (given by $\mu t = 1$) of 20 keV X-rays in most materials (atomic number > 20) is less than 0.1 mm. By using higher energy X-rays it can be increased to 1 mm for iron at 60 keV for example and several millimetres at 100 keV . The advantages of a much higher penetration are that it enables measurements to made deep inside thick samples or. alternatively. from small samples surrounded by packing material as in the high pressure cell described in Section 4.2.

3.3 - Sensitivity to Lattice Parameter Changes

For a given fractional change in the lattice parameter of the material. induced by a change in pressure. temperature or the presence of a residual strain for example. the *'relative '* change in lattice parameter $\Delta d/d$ is related to the relative change in energy $\Delta E/E$ through the expression

$$\frac{\Delta d}{d} = -\frac{\Delta E}{E} .$$

(5)

obtained by differentiating (1) whilst keeping θ constant. This shows that in EDXRD a given value of $\Delta d/d$ causes the largest shifts in the positions of the reflections at high energies. The condition expressed by (5) is obviously also valid for adjacent reflections corresponding to d-spacings separated by Δd. Their separation ΔE will be largest at high energies. This increase in the sensitivity of measurements of lattice paramenter changes at high values of E is an important advantage of this technique which will be exploited here.

3.4 - The Relative Energy Width

The expression for the relative FWHM of a reflection $\Delta E_T/E$, obtained by dividing expression (2) by E, is

$$\Delta E_T/E = \left[\frac{k_1}{E^2} + \frac{k_2}{E} + k_3 \right]^{1/2} \quad . \tag{6}$$

This expression shows that the relative energy widths of the reflections will decrease with increasing energy, as k_1, k_2 and k_3 are all positive (Section 2), and thus the resolution will increase. This is a potentially important advantage of using high energy X-rays, but in order to exploit it fully, it needs to be looked at in wider context as we shall now see.

3.5 - Optimum Resolution and Choice of Geometry

The resolution is the ability to separate two peaks with widths ΔE_T and a distance dE apart, and in practice it is strongly dependent on k_3, that is on the experimental geometry. Once a detector has been acquired k_1 and k_2 are fixed (Section 2), but k_3, which is equal to $(\cot\theta\Delta\theta)^2$ may be adjusted to give the optimum resolution within the constraints of the experiment. Various techniques can be used to choose the values of θ and $\Delta\theta$. They are not straight forward and rarely do they give a clear-cut answer.

The widths of the reflections can be kept low by reducing the geometrical broadening. This may be achieved by working at high angles of diffraction, to reduce the magnitude of $\cot\theta$, at low energies and with small beam divergences. The latter is dependent on the size and brightness of the source, whilst the others conflict with the feature discussed in Section 3.3, that is a larger separation between adjacent peaks at high energies and thus low angles of diffraction. If we choose the condition for resolution to be

$$\delta E_{FWHM} \doteq \Delta E, \tag{7}$$

where δE_{FWHM} is the mean width of two adjacent reflections separated by ΔE, then if the sample has a high enough crystalline symmetry, the resolution will be adequate at all values of θ larger than a few degrees.

This is illustrated in **Figure 1** where the quantity $\Delta E/\delta E_{FWHM}$ is plotted as a function of θ for the first 9 reflections in the spectrum of silicon. In each case δE_{FWHM} and
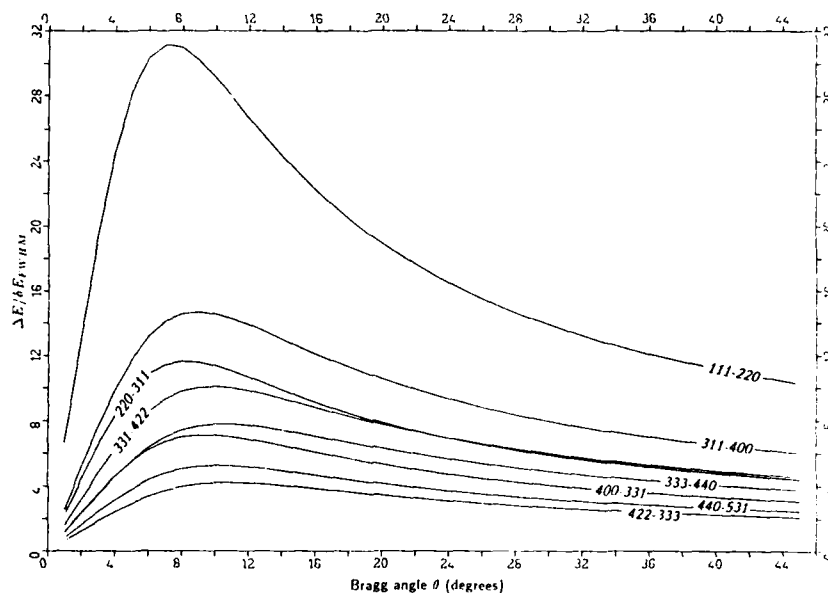
Figure 1 - Calculated resolution for the spectrum of silicon. ΔE is the separation of a pair of reflections. δE_{FWHM} their mean width

ΔE are the mean width and separation, respectively, of two adjacent reflections expressed on the energy scale. The values of δE_{FWHM} were calculated using expression (2) and the values of k_1, k_2 and k_3 applying to the experimental conditions described in the Section 5.1. The curves show that although the function has a maximum of approximately 31 at 7" for the *111-220* pair and 4 at 11° for the *422-333* pair. its value is larger than 1 for all values of θ greater than 2° and decreases at values of θ larger than approximately 12° degrees. This approach demonstrates that with the kind of collimation achievable in a conventional laboratory setup. the choice of θ and $\Delta\theta$ is not straight forward. In the work presented here the value of $\Delta\theta$ was fixed to 5×10^{-3} *radians* by the source size and the need to place the sample reasonably near the source as the high voltage generator does not have a very high brightness. With the kind of resolution achievable with synchrotron radiation $(\Delta\theta \cong 10^{-4}$ *radians*) the maxima are very sharp and occur at approximately 5" and in this case the choice is straight forward.

In the light of the above discussion. it can be seen that the final value chosen for 2θ has to be a compromise between resolution and intensity. It needs to be made in

consideration of the symmetry of the material studied and is therefore best investigated experimentally. This approach was adopted in the work reported here.

4 - Experimental Setup and Technique

4.1 - The Diffractometer Arrangement

As the high voltage generator was built for radiography work, the shielding of its X-ray tube was not suitable for standard laboratory use in the proximity of an experimenter or detector. The tube was therefore enclosed in a brass cylinder lined with 8 mm thick lead and attached to the simple experimental setup shown in **Figure 2**.

The first stage of the collimation system consisted of a tungsten plug screwed into the wall of the tube shielding and limiting the vertical divergence of the incident beam. The horizontal divergences of the incident and diffracted beams were limited by 10 cm long blocks of molybdenum inserted into stainless steel supports. These molybdenum *parallels* had finely ground surfaces separated by 0.2 mm spacers. The first set of parallels was fixed to the tube housing, whilst the second set was mounted on a low accuracy rotary table in order to facilitate the setting of the scattering angle. Both sets of parallels could be finely rotated in the plane of diffraction and translated in a direction perpendicular to the X-ray beams to facilitate the alignment of the diffractometer system.

The vertical divergence of the diffracted beam was limited by a set of 5 cm long Soller slits. They consisted of 20 strips of 0.15 mm thick molybdenum mounted between two blocks of brass at a pitch of 0.7 mm. At the small scattering angles required by high energy X-rays, the curvature of the cone of diffraction is very high and Soller slits are indispensable. The use of molybdenum for the parallels and Soller slits ensured that the effective collimation did not vary with energy. Safe shielding was achieved by enclosing the complete collimation system in a simple double-walled castle made of 3 mm thick lead.

4.2 - The High Pressure Cell

The high pressure cell is shown in **Figure 3**. Its dimensions and details of its components are given in the diagram of **Figure 4**. The polycrystalline sample is placed
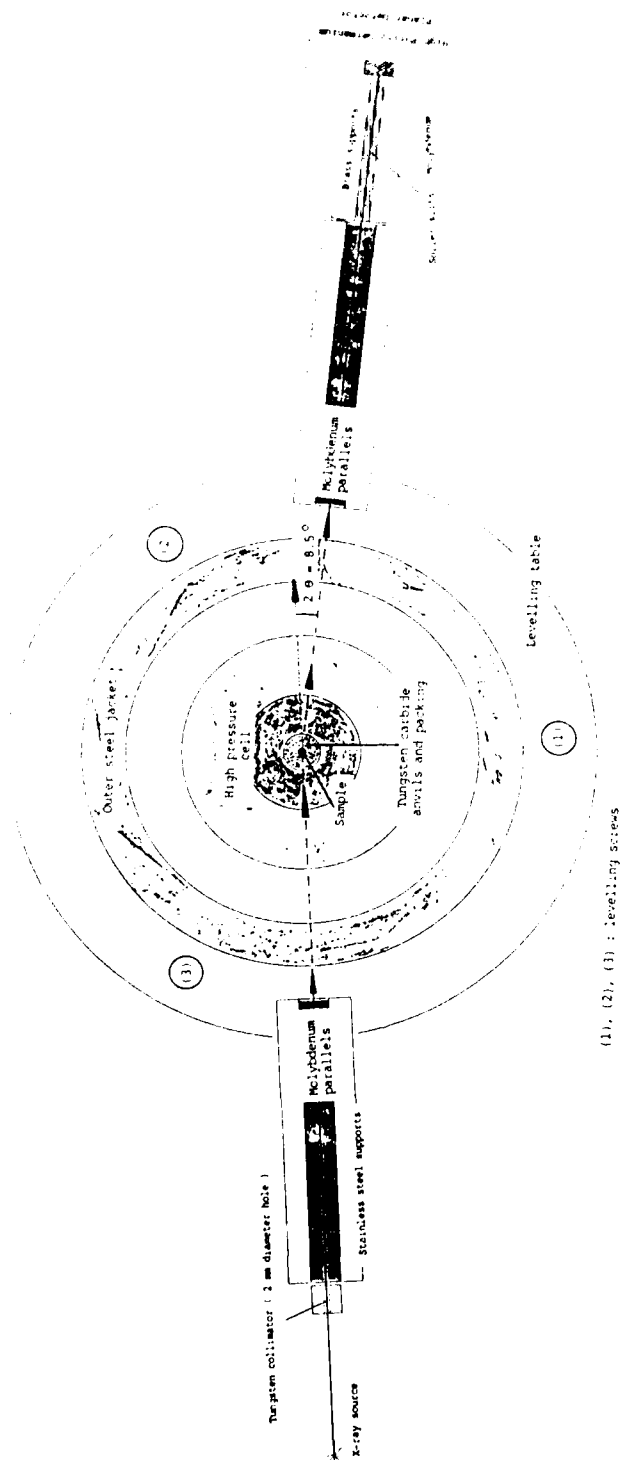
Figure 2 - Experimental arrangement. The diffractometer with the high pressure cell assembly

Divergences Horizontal (in plane of diagram)   Incident beam   3.2 mrad
                                                  Diffracted beam 4.0 mrad

             Vertical   Incident beam   27 mrad
                                                  Diffracted beam 22 mrad

Source size   0.4 mm

Source to sample distance   28.5 cm

Sample to detector distance   27.5 cm

Distance between the parallels   20 cm

Source to tungsten plug distance   9 cm

(1), (2), (3) : levelling screws
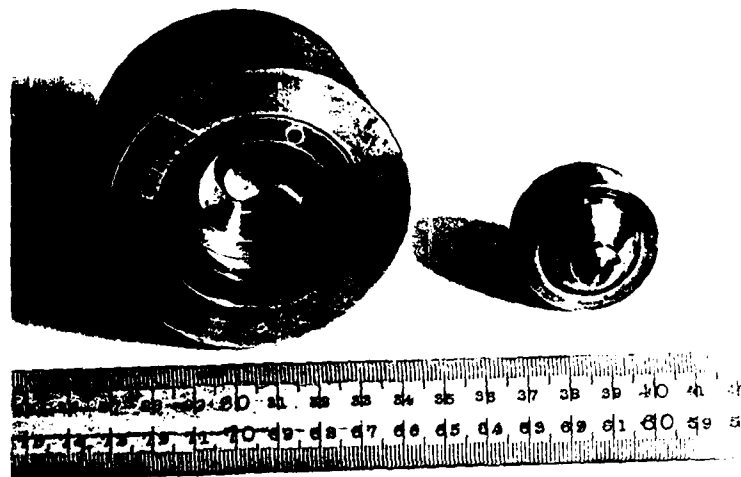
Figure 3 - The Drickamer-type high pressure cell used for our measurements. The windows for the direct and diffracted beams are machined for $2\theta = 8''$. Pressure is applied onto the 12.7 mm tungsten carbide anvils using a 12 cm diameter steel piston An oil pressure of 7,000 *psi* generates a final pressure of approximately 130 *kbar* across a 0.25 mm thick sample located at the center of the anvils.

in a small hole at the centre of the disc of packing which acts as a pressure vessel. The pressure is applied by compressing the disc between two tungsten carbide anvils supported by tight fitting tapered cylinders machined from tool steel.

In the design used here the anvils are tapered with a small flat 2 mm in diameter at their centre and the packing is contained within a doubly tapered ring of tool steel (Figure 4). When the pressure is applied, the centre is compressed much more than the taper. The pressure across the flat is approximately constant whilst a pressure gradient exists between the edge of the flat and the outside edge of the anvils. The greater the taper, the higher the gradient and thus the higher the maximum pressure at the centre. but also the higher the tendency for the sample to extrude from the centre flat. In the present design. we have optimised both these conflicting factors by reducing extrusion using a small initial taper of 6'' and increasing the containment pressure of this central ring by a second taper of 20''. The basic principles used in this design are those of 'massive support' and 'cells within a cell'. Both can be understood by visualising the central part of the cell as an assembly of concentric cylinders within which each cylinder with radius r contains its neighbour with
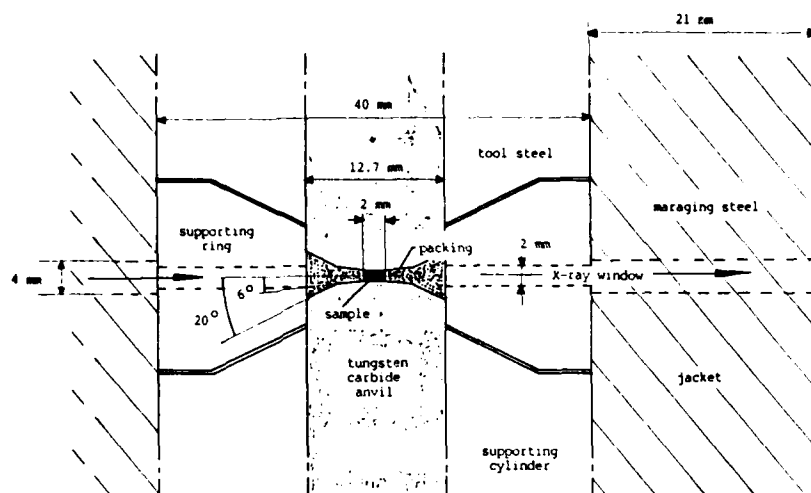
Figure 4 - Diagram of the high pressure cell. The section is through the axis of the cell The windows are offset by 8" with respect to one another in the plane perpendicular to that of the diagram.

radius $(r - \delta r)$. In the case of the anvils, this process prevents them from breaking under the very high pressure existing in their centres. This is the principle of *massive support* The packing also participates in this process by supporting the anvils along the tapers The packing is under a continuously decreasing pressure from the centre outwards and contains itself by the principle of *cells within a cell*. This minimises extrusion from the centre and thus allows the use of reasonably large samples. It also ensures that the average pressure applied on the anvils and the drop in pressure at their edges are such that extrusion of the packing into the windows for the X-ray beams is minimised. The maximum pressure at the centre, P_c, will be a function of the distance between the central flats, t For a cell with 12.7 mm diameter anvils, a single 6" taper and NaCl packing, the following empirical relationship exists between the above parameters and the applied pressure P,

$$P_c = P_a \left(1 + \frac{0.525}{P_a^{0.25} \, t^{1.25}} \right)$$

Here the pressures are in *kbar* and t_c in *millimetres*. **Figure 5** shows the variation of P_c as a function of t_c calculated using the above equation for a constant applied pressure P_a of 36 *kbar* : this value of P_a is close to the maximum pressure which can be applied to the anvils before fracture occurs. The improvement in performance achieved with the present

13
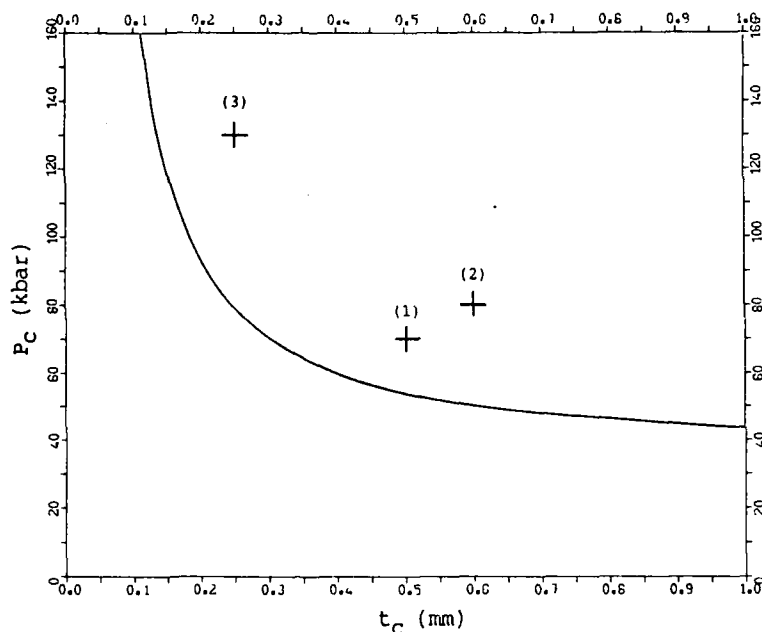
Figure 5 - Performance of the high pressure cell. The curve was calculated using equation (8). It shows the pressure P_c at the centre as a function of the anvils separation t_c for a constant applied pressure P_a of approximately 36 *kbar*. (see text for comments on (1). (2) and (3).

cell are also illustrated in Figure 3.3. The point labelled **(1)** was obtained using NaCl as packing material and shows that the addition of a 20'' taper improved the performance by approximately 30%. The point labelled **(2)** was obtained during the measurements reported below. The packing was a mixture of 50% LiF and 50% epoxy which has a greater shear strength than NaCl and thus further improves the performance. It also has the advantage of lower absorption of X-rays. Drickamer was limited in his choice of packing materials as his measurements were made optically and thus the packing had to be transparent. The point labelled **(3)** was obtained during the work with synchrotron radiation presented in Section 5.3. The much higher intensity of the radiation enabled the use of smaller samples and thus smaller values of t_c.

The central cell assembly, made up of the anvils, thei supporting cylinders and the central ring containing the packing, was surrounded by a tight fitting jacket of maraging steel (Figures 3 and 4). The entire cell was placed between two tungsten carbide pads with

diameters of 2.5 cm and inside a 15 cm diameter steel jacket. The outer jacket, which had 1.5 cm thick walls, contained a 12 cm diameter hydraulic piston. Pressure was generated manually using a oil ram, and an oil pressure of 7,000 *psi* (approximately 5×10^7 *Pa*) was required to produce the maximum safe applied pressure of 36 *kbar* on the tungsten carbide anvils.

4.3 - Experimental Technique

The cell and its steel jacket were placed with their axis aligned with that of the diffractometer (Figure 2). They were mounted on a steel table, the height and tilt of which could be adjusted using three levelling screws. This provided enough degrees of freedom to bring the plane of the small disc of sample into that determined by the X-ray source and the Soller slits.
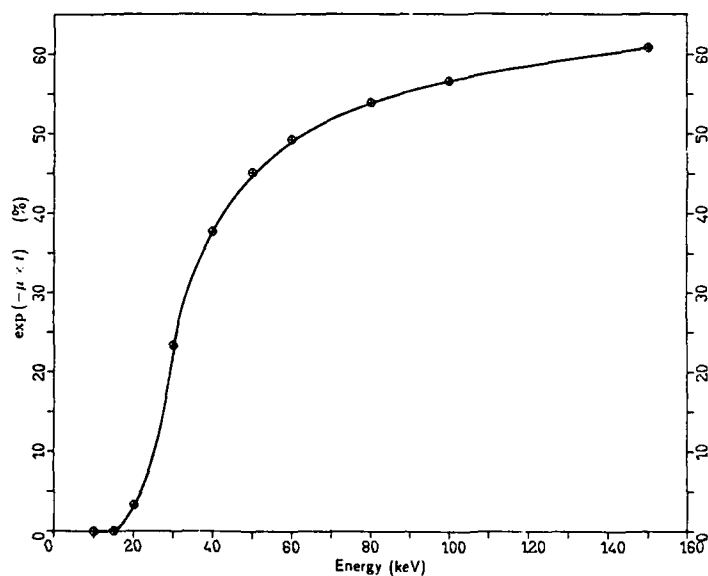

Figure 6 - The transmission of 15 mm of 50% LiF - 50% epoxy packing.

As Figure 2 shows, both the incident and diffracted beams had to travel through the packing and this made the use of high energy X-rays indispensable. This is clearly illustrated in **Figure 6** which shows the transmission of a disc of packing over the range

of energies of the high voltage generator. The effect of the sample has been ignored, the latter usually has a higher atomic number, but 1.25 mm of packing extrusion into each X-ray window has been included. If a 60 kV generator were to have been used, Figure 6 shows that the packing would have been almost totally opaque over half its useful range of energies.
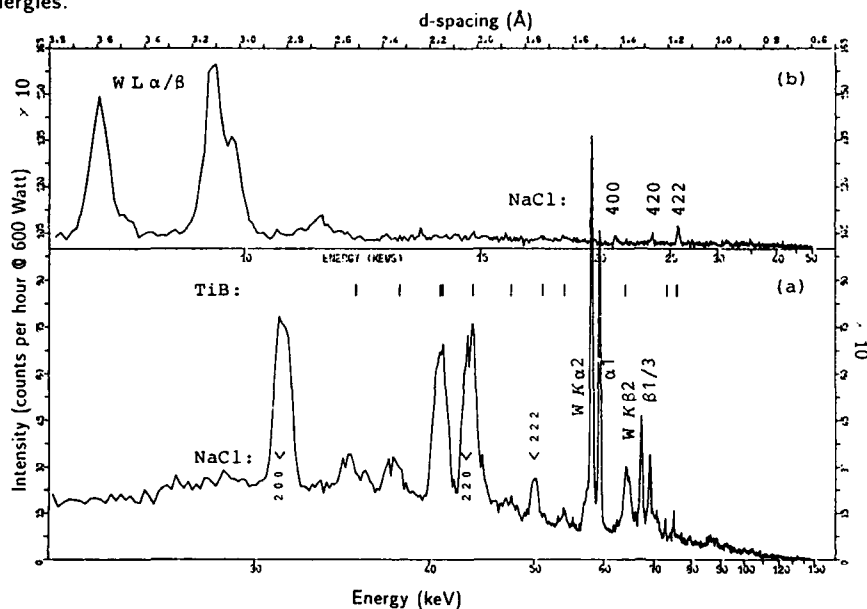
Figure 7 - EDXRD spectra of a composite sample of TiB and NaCl. (a) 150 kV and $2\theta = 8°$.(b): 50 kV and $2\theta = 24°$ (offset by 1000 counts)

Further evidence of the advantage of using high energy X-rays is provided by the spectra shown in **Figure 7**. Both were obtained using the **same** composite sample of TiB and NaCl, the replica of a sample used in the work presented below, but the lower spectrum (a) at $2\theta = 8°$ and 150 kV, while the upper specturm (b) was obtained using the conventional operating voltage of 50 kV at $2\theta = 24°$. The relative d-spacing positions were therefore preserved in the two spectra which have been normalised to the same tube power and data collection time. The sample consisted of two discs of TiB, each 1.8 mm in diameter and 0.5 mm thick, lying parallel to the plane of diffraction, separated by 1 mm of hand packed NaCl and placed in the centre of 12.5 mm of LiF-epoxy packing. In the low energy spectrum absorption was such that no peaks were obtained apart from those due to

elastic scattering of characteristic tungsten L radiation and the most energetic diffraction peaks from the NaCl disc. These latter were helped by the low density of the salt (probably 50% of the crystal density) but hindered by its low scattering power and small Debye-Waller factor at these values of d-spacing. In striking contrast the high energy spectrum shows a full diffraction pattern. The 50% LiF - 50% epoxy packing material was selected for its high shear strength (Section 4.2), low absorption and low scattering power. This last characteristic was very important considering the geometry of the collimation used here. The effective length of the incident and diffracted beams intersection was calculated as 7.5 mm. As the sample diameter was typically 1.8 mm, a large percentage of the intersection was located within the packing. In order to minimise the contribution of the latter to the final spectrum, it was thus essential to use a material with a low scattering power

The next material to be considered is the internal pressure calibrant. The latter a material with an accurately known compressibility, must be a good scatterer of X-rays with a simple structure. The number of overlaps between reflections from the sample and the calibrant has to be a minimum, and thus it is advisable to choose the calibrant by comparing its spectrum with that of the sample.

When the cell is assembled and placed on the diffractometer, it therefore contains a composite sample which is a mixture of sample and calibrant, and the packing material. The spectra are therefore complicated as they are a superposition of the three diffraction patterns of these materials. This is illustrated in **Figure 8** where an imaginary spectrum created by the addition and scaling of its three components, is compared with a real spectrum obtained during the measurements presented below. The final spectrum clearly indicates the need for the large dynamic range of the X-ray generator (Section 3.1) The prominent tungsten $K\alpha$ lines from the target were unfortunate and unavoidable but proved to be also useful. The low intensities diffracted by the smallest sample volumes, of the order of $1 mm^3$, required exposures of up to 12 hours. The position and width of the tungsten lines provided an excellent means of checking the stability of the detector system during these long exposures.

Figure 8 - **The composition of a spectrum.** (a). the packing with no sample: (b) copper. the pressure calibrant: (c) TiB. the sample on its own: (d) simulated spectrum. the normalised sum of (a). (b) and (c). (d) a real spectrum obtained from the packed cell at 0 *kbar*.
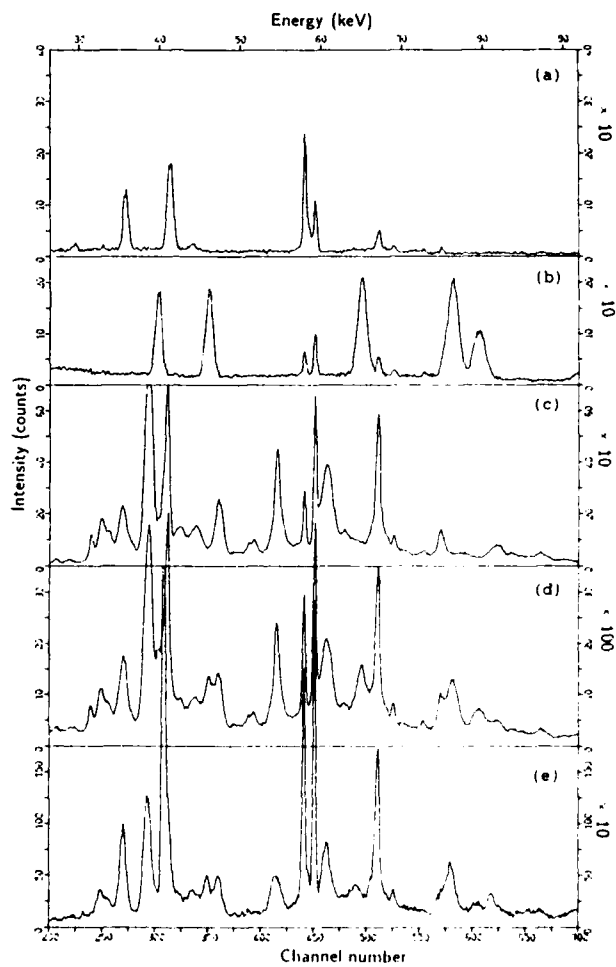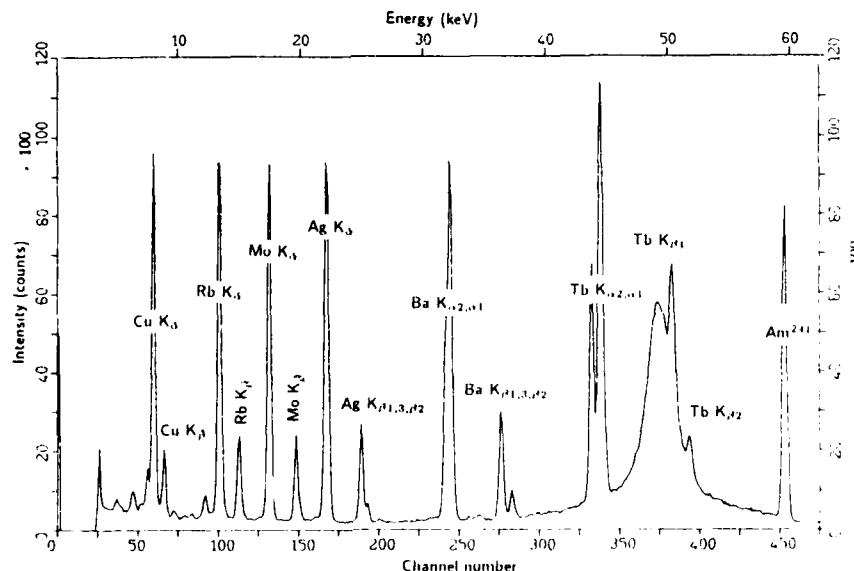
Figure 9 - Energy calibration spectrum obtained from a variable energy X-ray source

4.4 - Detector Systems, Energy Calibration and Data Analysis

Two detector systems were used in the work presented here. Each consisted of a high purity germanium planar detector. a spectroscopy amplifier and a multi channel analyser. The detector crystals were 5 mm thick. 10 mm in diameter for the work carried out with the high voltage generator and 13 mm thick. 16 mm in diameter for that carried out with synchrotron radiation. The latter was custom built by EG&G ORTEC and combined with state-of-the-art electronics. Its thickness ensured an efficiency of 100% up to 100 keV and the electronics a linearity in energy of 1 part in 10^1 compared to approximately 3 parts in 10^4 for the other system.

Energy calibration of the detector systems were performed using a variable energy X-ray source. Such a source uses the 60 keV γ-rays radiated by Americium[241] to excite characteristic X-rays from copper. rubidium. molybdenum silver. barium and terbium A typical spectrum can be seen in **Figure 9**.

When the resolution of the detector was not sufficent to separate the $K_{\alpha1}$ - $K_{\alpha2}$ and $K_{\beta1,3}$ - $K_{\beta2}$ doublets of the elements with low atomic numbers. the peaks were treated as single peaks and their energy taken as the intensity-weighted means of their various

components. The analysis of the calibration spectra was performed using a program based on a Gaussian fitting technique specially written for this task. The program automatically located all the peaks corresponding to the calibration line energies and fitted the sums of Gaussian envelopes and a sloping background to the appropriate sections of the data. The last stage of the analysis, also included in the program, consisted of two weighted linear least squares fits to the centroids and positions and widths and positions respectively, of all the calibration lines. The first fit was to the equation

$$E = p \cdot m + c, \tag{9}$$

where E is the energy of the line with position p channels, and produced the calibration slope m and zero offset c. The second fit was to

$$\Delta E_D^2 = \Delta E_{amp}^2 + 2.355^2 F \epsilon E,$$

(from expression (2)) which quantifies the intrinsic resolution ΔE_D of the detector system, and produced the two detector constants ΔE_{amp} and F (expression (3)).

After collection, all the spectra were sent from the analyser to a main frame computer, in that case a DEC VAX 11/780. The program, based on an iterative least squares fitting technique involving the linearisation of a non-linear function, was developed specifically for this work. It requires the operator to either input the first and last channel numbers of a region containing a single peak or the approximate positions and peak intensities of a number of peaks. The program is usually able to deconvolute peaks overlapping by up to 70% of their width when the difference in their intensities is smaller or equal to 90% of that of the largest peak. For peaks with equal intensities, the overlap can increase to 90%. The number of iterations is controlled by a *convergence criterion* of 0.01% which interrupts the fitting cycles when the adjustments of all the parameters being refined drops below that level. The program refines the height, width, and position of each peak, the slope and intercept of the background and calculates the integrated intensities and all the standard deviations. The refinement of 17 parameters, 5 peaks with 3 parameters each and 2 parameters for the sloping background, takes between 5 and 20 seconds depending on
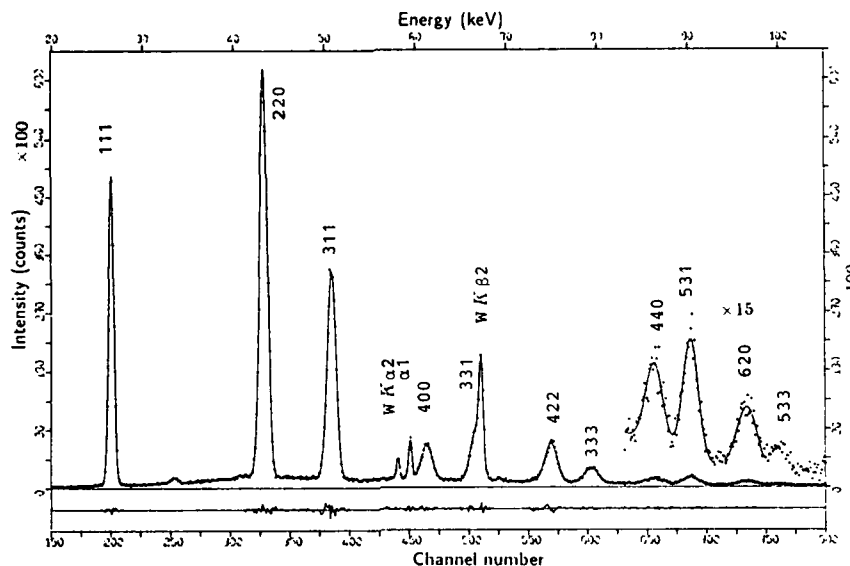
Figure 10 - **Energy dispersive spectrum of silicon powder collected at** $2\theta = 8.5°$. The sample was prepared from NBS Standard Reference Material 640a. The spectrum was obtained in 45 minutes at 125 kV and 5 mA using a tungsten tube. The fitted envelopes are 100% Gaussian and the differences between the latter and the data are plotted in the box below the spectrum.

the magnitudes of the overlaps. **Figure 10** illustrates the results obtained in the analysis of a silicon spectrum.

The accuracy with which the peak centroids were determined varies from less than 1 part in 10^4 for the three brightest reflections to 8 parts in 10^4 for the *533* reflection with a mean value of all the relative standard deviations of 3 parts in 10^4. The *331* reflection is a good example of deconvolution. It is partly made up of reflected tungsten K_{α_2} radiation from the target and overlaps by 80% the elastically scattered component of the line itself yet the accuracy of the deconvolution is of 6 parts in 10^4.

5 - Measurements and Results

5.1 - Compressibility Measurements and EDXRD

The effect of pressure on matter is to decrease its interatomic distances. If a polycrystalline sample is subjected to pressure, the change in its d-spacings can be measured

directly using X-ray diffraction. If the pressure P is established by some independent means, such as an internal pressure calibrant, then the compressibility of the sample can be calculated. An important parameter relating the change in volume to pressure is the bulk modulus at zero pressure, K_o. It is the inverse of the volume compressibility at $P = 0$ and is therefore given by

$$K_o = -V \left(\frac{\Delta P}{\Delta V} \right)_{P=0} \quad . \tag{10}$$

Compressibility measurements are thus differential measurements. They are concerned with establishing the change in the lattice spacings of the sample with pressure. In EDXRD, as the beams geometry is fixed, this involves only the measurement of the changes in the positions of the reflections on the energy scale, these shifts being measured with respect to the energies of the reflections at zero pressure. The relevant equation is therefore

$$\frac{\Delta d}{d} = -\frac{\Delta E}{E} \quad . \tag{11}$$

from (1), which shows that the scattering angle does not have to be known. The only source of errors in these measurements are therefore those associated with establishing the energies of the reflections. The two contributions to the latter are δE_D, the contribution from the linearity of the energy calibration of the detector system, and δE_S, that of the accuracy with which the centroids of the reflections can be determined. As these contributions are random errors, the final relative accuracy in E is given by

$$\frac{\delta E}{E} = \sqrt{ \left(\frac{\delta E_D}{E} \right)^2 + \left(\frac{\delta E_S}{E} \right)^2 } \quad . \tag{12}$$

With the data presented here, the value of the latter varied approximately from 8 parts in 10^4 for TiB inside the high pressure cell whilst working in the laboratory with the high voltage generator and the first detector system described above and 1 part in 10^4 with TiB_2 inside the cell with synchrotron radiation and the second system.

5.2 - Measurements on TiB

The titanium boride had been made by reaction sintering without binder under high temperature and pressure. It was found to be an extremely hard material and consequently the samples, in the shape of slices and small discs, had to be machined using diamond coated tools. The aims of the measurements described below were:

- to characterise this new material by comparing its diffraction pattern with that tabulated in the *JCPDS* file:

- to determine its compressibility and thus its bulk modulus K_o:

- to establish whether its behaviour under pressure would show any signs of a phase change.

In all the measurements described below the calibration of the detector system and the data analysis were performed in the manners described in Section 4.4.

5.2.1 - Characterisation of a New Material

EDXRD is intrinsically a low resolution technique which is best used for measurements on materials with a reasonably high crystalline symmetry. TiB has an orthorhombic structure with the space group *Pnma* - D_{2h}^{16} and it is thus impossible to measure a sufficiently large number of d-spacings to characterise this material with the present technique as both the brightness of the source of radiation and the resolution are too low. We shall see in the next section that this technique is adequate for compressibility measurements. but in order to measure the positions of a large number of reflections. both the resolution and statistics have to be considerably increased. Consequently. the measurements reported below were made with synchrotron radiation. As the experimental arrangement used for these measurements will be described in some detail in the next section we shall only say here that the resolution and diffracted intensities increased by factors of approximately 2.5 and 1000 . respectively. and that the high energy radiation from the 'Wiggler' was used.

The diffractometer was calibrated using the diffraction spectra obtained from samples with accurately known lattice parameters. This calibration was performed twice. Once using a free standing sample of high quality silicon powder (NBS SRM 640a) and once using a disc of copper foil inside the high pressure cell with no pressure applied. Both calibrations were found to be in very good agreement although small variations of the scattering angle with energy were observed in both cases. As the low symmetry of the structure of TiB and its small scattering power did not allow quite as high an accuracy as that obtained in measurements on samples with cubic structures. these small variations were ignored and
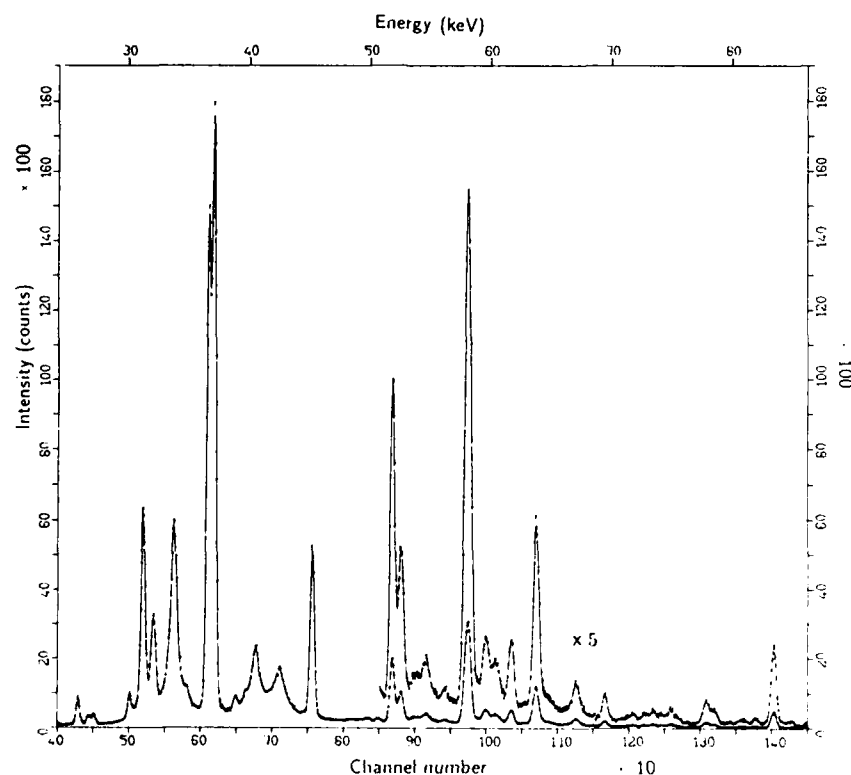
Figure 11 - EDXRD spectrum of TiB obtained using Synchrotron Radiation. This spectrum was collected in 45 minutes from a 1 8 mm thick sample at $2\theta = 9^\circ$ Wiggler radiation was used and the machine parameters were 2 *GeV* 150 *mA* and 5 *Tesla* (see Section 5.3 1) The Gaussian envelopes were calculated using the technique described in Section 4 4

the mean of all the values of the Bragg angle obtained from the brightest reflections in the two spectra was used as the calibration. This mean value was calculated as

$$\theta = 4.4857 \pm 0.0013$$

The relative error introduced by this calibration in the d spacing measurements was approximately

$$\delta d/d = 3.0 \times 10^{-4}.$$

The measurements were made in transmission from a 1.8 mm thick slice of the material. The spectrum is shown in **Figure 11** Neither the technique used here nor the

Table 1 - The d-spacings of TiB.

$d(\mathring{A})$ PDF	$d(\mathring{A})$ meas.	$\delta(d) \cdot 10^3$	Comments
3 053	3 0645	13	-
.	2 6330	11	TiB_2
2 543	2 5406	10	.
.	2 4720	11	unknown
2 346	2 3484	10	.
2 161	2 1651	9	
2 140	2 1394	9	
.	2 0413	10	$(TiB_2 ?)$
1 956	1 9568	10	.
1 863	1 8649	13	.
1 755	1 7536	8	.
1 528	1 5294	7	.
.	1 5088	7	$(TiB_2 ?)$
1 461	1 4511	8	.
1 362	1 3650	7	.
1 331	1 3305	7	.
1 310	1 3122	8	.
.	1 2851	7	unknown
1 244	1 2439	6	
1 181	1 1819	7	.
1 141	1 1414	6	
1 017	1 0182	6	.
1 008	1 0093	7	
0 949	0 9498	6	.

purity of the sample were sufficient to perform a structure refinement. The alternative was to measure the d-spacings of as many reflections as possible and compare them with those given in the Powder Diffraction Files (PDF). These results are shown in **Table 1**. As the values of δd show, the agreement between the two sets of values is within the present experimental error. The average relative accuracy achieved in the data analysis was approximately

$$\frac{\delta E}{E} \qquad 10 \quad 10^{-3}$$

which combined with the contribution from the diffractometer calibration to give a final accuracy in $\delta d/d$ of approximately 5 parts in 10^3 as the values of δd indicate.

The d-spacings labelled TiB_2 did not match any of PDF values but agreed with strong reflections in the spectrum of TiB_2 (see Section 5.3.2). Those labelled *unidentified* belonged to neither compound. The presence of TiB_2 in TiB is plausible as both compounds

were made in a similar manner but TiB_2 at a higher temperature. When other spectra were collected from different parts of the same sample and along different orientations using other samples with the same thickness. the relative intensities of the reflections. both TiB-TiB and $TiB-TiB_2$. were found to vary appreciably. This indicated the presence of both preferred orientations, to be expected considering the technique used to make the material. and an inhomogenous distribution of the two compounds. The accuracy of the present measurements was however not sufficient to quantify these observations.

5.2.2 - The Compressibility of TiB

The measurements at high pressures. made at $2\theta - 8.5''$. were divided into two sets. In the first set the sample assembly consisted of two 0.5 mm thick slices of TiB separated by a few tenths of a millimetre of NaCl. the pressure calibrant. In the second set a 0.45 mm thick slice of TiB was placed between two 0.1 mm foils of copper. In both cases the diameters of the slices and foils were approximately 1.8 mm. When using the larger sample with NaCl. exposure times were of the order of 1 to 2 hours and the maximum pressure attained was 35 *kbar*. This upper limit was caused by the disappearance of the NaCl lines as the salt was squeezed out by the much harder TiB. The measurements made with copper and the smaller sample required exposure times which varied from 6 to 12 hours for the highest pressures. The maximum pressure of 80 *kbar* was limited in this case by the exposure time and the availability of the generator.

Four spectra obtained during the high pressure measurements on TiB are shown in **Figure 12**. With NaCl as the pressure calibrant. both the *200* and *220* reflections were used to determine the pressure. With copper. the *111* . *200*. *220* and *311* reflections were used over most of the pressure range covered. Figure 12 clearly shows that it was not possible to extract the three lattice parameters of TiB from such spectra as only three or four sets of reflections could be analysed. Consequently. the measurements were those of the *average linear compressibility*' The results of these measurements are given in **Table 2**. The reduced parameter is $\overline{d/d_o}$. which is the mean value obtained from the various sets of reflections. Throughout the range of pressures from 0 to 80 *kbar* and within the resolution and statistics of the present measurements. no sign of a possible phase transition were

Figure 12 - **EDXRD spectra of TiB at various pressures.** The spectra at 19 25 and 35 *kbar* were collected in 180 minutes at 150 *kV* and 4 *mA* Those at 8 8 and 55 7 *kbar* were collected in 360 minutes at 125 *kV* and 5 *mA* The scattering angle was $2\theta \simeq 8.5°$ The vertical lines indicate the shifts of the reflections with pressure
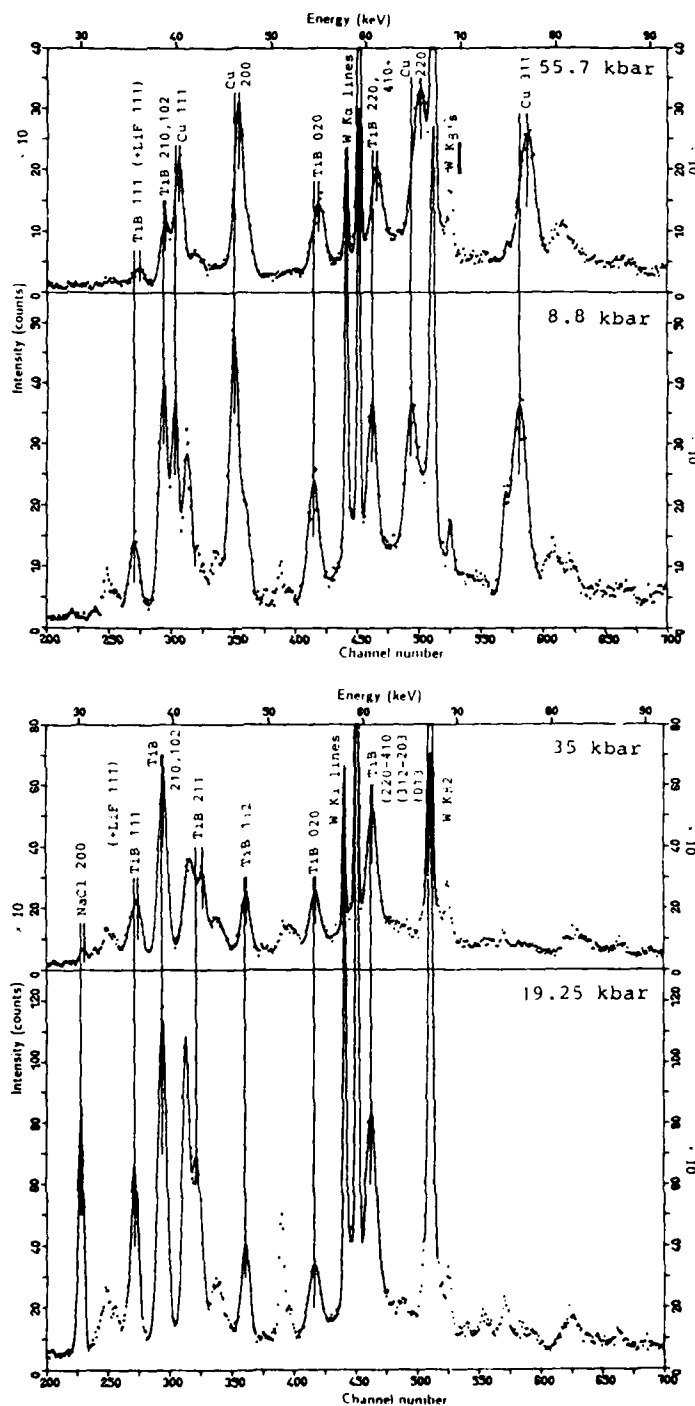
Table 2 - Average compressibility data for TiB.

$P(kbar)$	$\delta P(kbar)$	$\overline{d_i/d_o}$	$+\delta\left(\overline{d/d_o}\right) \times 10^4$
6.7	0.3	1.00053	2.4
14.9	0.3	0.99958	2.3
19.3	0.5	0.99971	2.0
20.4	0.6	0.99901	2.5
24.9	0.8	0.99774	2.3
25.5	0.8	0.99723	2.9
35.0	1.2	0.99602	1.6

NaCl as pressure calibrant

8.8	1.7	1.00068	1.8
22.0	1.8	0.99936	3.8
26.7	1.2	0.99776	3.7
38.3	1.5	0.99545	2.7
47.3	1.3	0.99478	3.1
55.7	1.5	0.99341	3.6
63.0	1.7	0.99165	3.1
78.8	1.9	0.98900	5.0

Copper as pressure calibrant

detected. As TiB was found to be not only extremely hard during machining. but relatively incompressible as well (see below). this was not unexpected.

The compressibility data obtained are plotted in **Figure 13**. The effect which caused the intercept to be larger than *1.0* was initially thought to have been due to a physical property of the material. The latter could have caused an inhomogenous compression. which appeared as a dilation in the direction perpendicular to the planes which d-spacings were being measured. However. once the measurements were completed. a close inspection of the packing throughout its thickness showed that it contained some air bubbles. This probably introduced a '*sponge effect* ' during the initial stage of the compression. which led to a considerable uniaxial component. Such a component would cause the effect described above in such a hard material. The slices of TiB would in fact act as small anvils. compressing the pressure calibrant. while dilating slightly themselves in the direction perpendicular to that of the uniaxial component. which is that of the d-spacings being measured. As soon as all the voids would have been squeezed out of the packing. the cell would have then behaved as expected. As measurements on the same sample with a new packing and synchrotron radiation showed no sign of this effect. it can be assumed that the above explanation is reasonable.
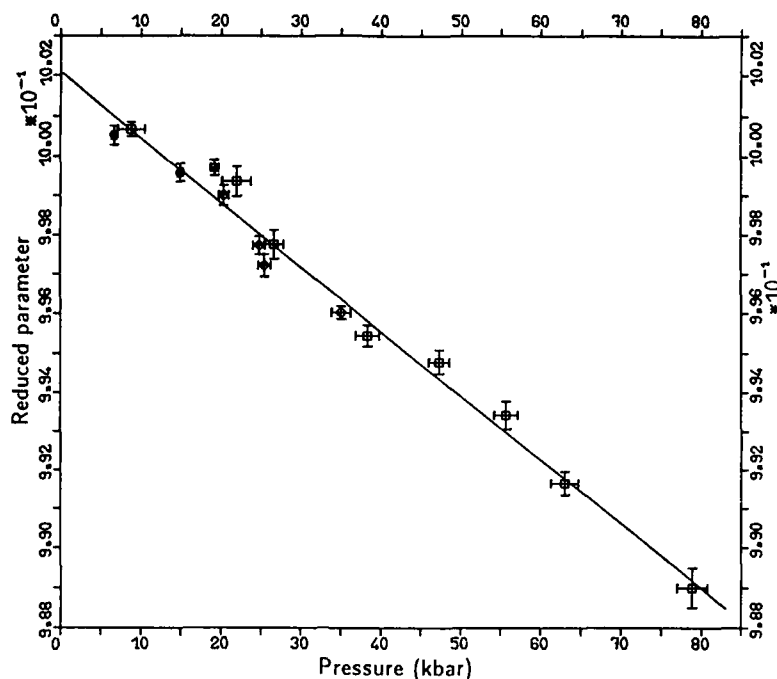
Figure 13 - Reduced parameter as a function of pressure for TiB. The reduced parameter. d/d_o. is the mean value calculated from the *111. 210. 102. 112. 020 and 220/410/+* reflections. The straight line is the result of a least squares fit to the data. The points indicated by *diamonds* were obtained using NaCl as the pressure calibrant. Those indicated by *squares* were obtained with *copper*.

The bulk modulus K_o of a material (Section 5.1) is usually determined by refining an EOS to its measured volume compressibility data. Considering the relative incompressibility of TiB. the small pressure range covered and the magnitude of the error bars in Figure 12. such an analysis is not justified here. Instead. K_o can be estimated to a good approximation from the gradient of the straight line fitted to the data (Figure 12). If we approximate the unit cell volume by $\bar{d}^3$. where $\bar{d}$ is the average lattice parameter from which the reduced parameter was calculated. then we can write

$$\overline{K}_o = -\frac{d}{3} \left(\frac{\Delta P}{\Delta d} \right)_{P=0} \qquad . \tag{13}$$

This expression shows that the average bulk modulus K_o is given by

$$\overline{K}_o = \frac{1}{3}(m)^{-1}. \tag{14}$$

where m is the gradient of the straight line of Figure 12. Performing this calculation yields

$$\overline{K}_o = 2.03 \pm 0.15 \quad Mbar,$$

for TiB. This value is a good approximation of K_o, but may be regarded as an upper limit since we have treated the relationship between d/d_o and P as linear.

5.3 - Measurements on TiB$_2$

5.3.1 - Synchrotron and Wiggler Radiation

SRS : $E_e = 2$ GeV

$\Psi \cong 0.25$ mrad

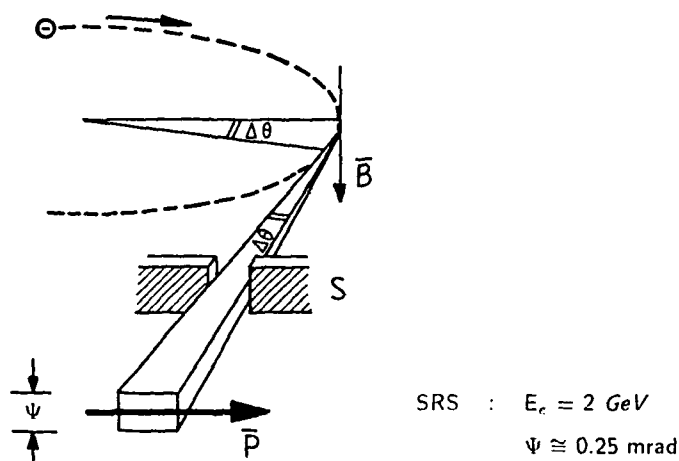Figure 14 - Synchrotron radiation emitted by relativistic electrons travelling in a circular orbit. B is the magnetic field perpendicular to the horizontal orbit plane. Ψ the natural collimation in the vertical plane and P the polarisation vector The slit S defines the length of the arc. corresponding to $\Delta\theta$. from which the radiation is taken.

The principle of the generation of SR is illustrated in Figure 14. When the electrons are relativistic and the source is a storage ring dedicated to the production of radiation as a research tool. the main properties of the radiation produced are:
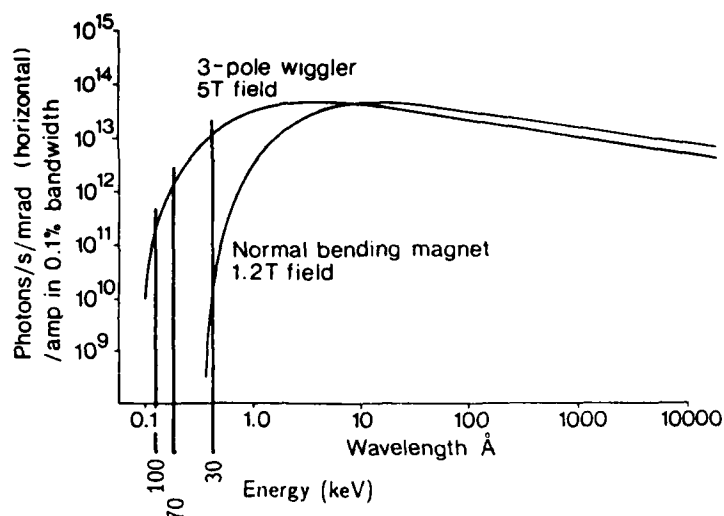
- a very high spectral brilliance;

Figure 15 - **Theoretical spectra of the SRS operating at 2 GeV.** Only Wiggler radiation is suitable for use with the Drickamer-type cell as the latter transmits only 1% of the incident radiation at 30 keV. The fast decreasing intensity of the Wiggler spectrum with increasing energy. a factor of 10 from 30 to 70 keV and a further factor of 10 from 70 to 100 keV. is a characteristic feature of all the diffraction spectra presented below

- a natural collimation in the plane perpendicular to the electron's orbit (the vertical plane) of the order of 10^{-4} *radians*;

- 100% linear polarisation in the plane of the orbit.

SR is emitted in the forward direction within a very small cone tangent to the orbit. For any point along that orbit the natural opening of the radiation fan in the horizontal plane is given by $2\sqrt{1 - \beta^2}$ where β is the ratio of the electron velocity to the speed of light in vacuum. The natural collimation Ψ in the plane perpendicular to the orbit is defined as the angular FWHM of the beam and is approximately given by

$$\Psi = \gamma^{-1} \quad \text{with} \quad \gamma \quad \frac{E}{m_e c^2}.$$

$m_e c^2$ being the rest mass energy of the electron. 0.511 GeV. The natural collimation is thus inversely proportional to the electron energy E_r. The United Kingdom Synchrotron Radiation Source (SRS) has a maximum electron energy of 2 GeV which gives $\Psi \simeq 0.25$ *mrad.* For comparison. a typical experimental collimation used with a standard X-ray source would be 5 *mrad* .

The *spectral flux* of the SRS is shown in **Figure 15** It is defined as the number of photons emitted per second in a given bandwidth within 1 *mrad* in the plane of the orbit and integrated in the vertical plane. In the X-ray region of the spectrum, the source dimensions of the SRS operating at 150 *mA* and 1.8 *GeV* of electron current and energy, respectively, are 0.25 mm and 12 mm in the vertical and horizontal planes, respectively, which give an effective source area of 3 mm^2 The position of the continuous spectral distribution of radiation on an energy scale is defined by the characteristic energy E_c which divides the spectrum into two equal parts of radiated power. It is given by

$$E_c - 2.22 \frac{E_e^3}{R} \quad 0.665 E_e^2 B. \tag{15}$$

where R is the radius of curvature of the electron path caused by a magnetic field B. The SRS operating at an electron energy E_e of 2 *GeV* has a critical energy E_c of 3.19 *keV* with a dipole magnetic field of 1.2 *Tesla*. The maximum energy at which the spectrum cuts off is also proportional to E_e^3/R (or $E_e^2 B$), and as Figure 15 shows it is approximately 30 *keV*. This makes the radiation produced by a normal bending magnet unsuitable for the high pressure work proposed here as the Drickamer-type cell described in the previous chapter has an effective cut-off in transmission at approximately this energy (Figure 6). However, as expression (15) indicates, the spectrum can be shifted towards higher energies by increasing the magnetic field B whilst preserving the same electron energy. This is achieved at the SRS by using a wavelength shifter, or *Wiggler*, the spectrum of which is also shown in Figure 15. The spectral flux produced by this device still falls off sharply at high energies, a factor of 10 between 30 and 70 *keV* and a further factor of 10 between 70 and 100 *keV*, but nevertheless produces useful intensities up to 124 *keV* (0.1 Å).

The principle of such a device is illustrated in **Figure 16** The SRS Wiggler has a central coil which produces a field of 5 *Tesla* in the downwards direction and two outer coils with fields of 3 *Tesla* in the upwards direction Placed on a straight section of the orbit between two dipole magnets, it forces the electron beam to describe a *wiggle* with a central radius of curvature of 1.3 m. The radius of the electron orbit in the conventional 1.2 *Tesla* dipoles is 5.6 m.

The low cost diffractometer designed and built for the work presented here is shown in **Figure 17**. Its concept is similar to that of the experimental setup described in Section
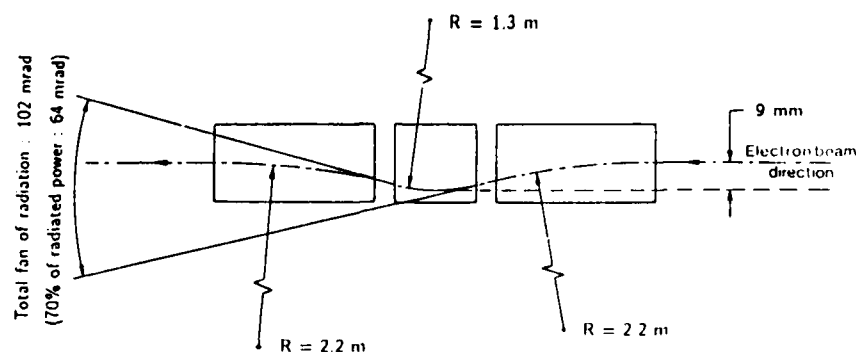
Figure 16 - Schematic diagram of the beam geometry inside the SRS Wiggler.

4.1. but modified for use with SR. The molybdenum parallels are mounted on a rigid stainless steel optical bench and supported kinematically in only two points which positions were calculated to minimise deformation under gravity. Combined with appropriate cross-section profiles. this guarantees deformations to be less than 0.2 μm. The scattering angle is set by altering the height of the end of the optical bench furthest from the cell using a vertical screw with a pitch giving aproximately 0.15" per turn. The principle of the diffractometer is to move the beams rather than the cell. for convenience. as the cell assembly weighs approximately 25 kg. In order to minimise the quantity of background radiation reaching the detector the two sets of incident beam slits were designed to plug into one another and all air paths were kept to a minimum. The incident beam was enclosed in a lead box from the beam pipe window to the cell and the thick steel walls of the latter and its jacket contained all the radiation scattered by the sample and packing

5.3.2 - The Compressibility of TiB$_2$

The samples consisted of thin discs. approximately 1 5 mm in diameter. which had been machined using diamond-coated tools as TiB$_2$ is a very hard material. The pressure calibrant was copper and the packing a mixture of 50% epoxy. 50% LiF (Section 4.2). The thicknesses of the copper foils were either 50 or 100 μm and those of the slices of TiB$_2$ varied between 110 and 140 μm. Most of the measurements were made using a 450 μm
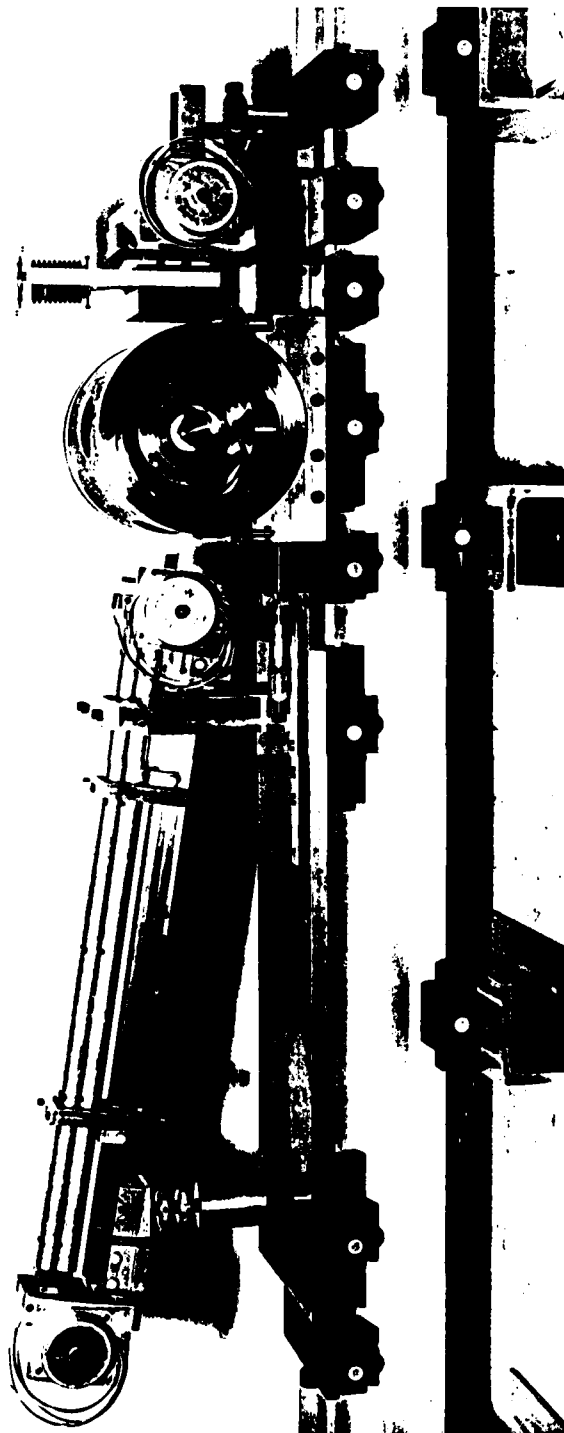
Figure 17 - The diffractometer with the high pressure cell. It is designed to operate at a fixed scattering angle 2θ between 6' and 10''. Two tungsten carbide slits, located on the right-hand side of the 15 cm diameter steel jacket limit the horizontal and vertical divergences of the incident beam. The cell itself is in position inside the jacket with one of its anvils removed and displayed in the forground. The vertical divergence of the diffracted beam is controlled by the two 50 cm long molybdenum parallels which can be seen on the left of the cell assembly between another pair of tungsten carbide slits. That located furthest from the cell limits the horizontal divergence, whilst the other acts as an anti-scatter slit. All slits are motorised for remote-control but the angle of diffraction is set manually.
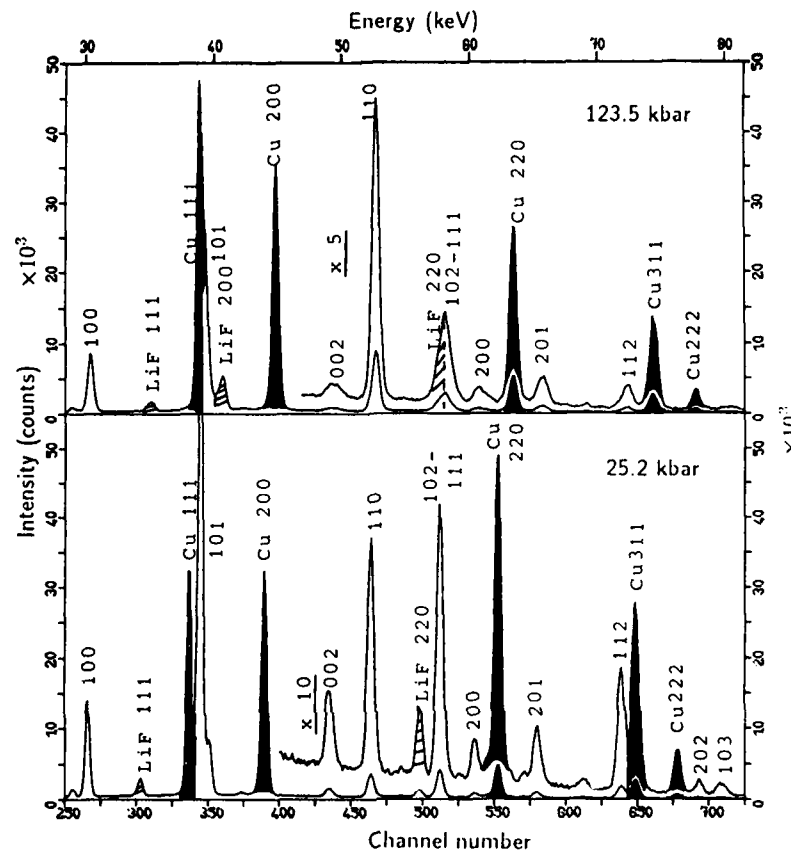
Figure 18 - Energy dispersive spectra of TiB$_2$ obtained with Wiggler radiation at $2\theta \cong 9°$. The spectrum at 25 2 kbar was collected in 25 minutes. that at 123 5 kbar in 45 minutes. The SRS was operating at 2 GeV and a current varying from 300 to 100 mA. The pressure was calculated from the copper reflections. shown in black and the peaks labelled only 'hkl' belong to TiB$_2$ The low intensity reflections from LiF indicate a small contribution from the packing

thick sample assembly. The maximum pressure of 130 $kbar$ was obtained after a reduction of the thickness to 290 μm. Two spectra are shown in **Figure 18** Both the signal-to-noise ratio and the resolution are very good. In addition. the combination of the high energy radiation from the Wiggler with a low Bragg angle of 4.488'' ensure that useful intensities are available up to 80 keV. The divergences were 0.04 $mrad$ and 0.8 $mrad$ for the direct and diffracted beams. respectively. and the slit separations were 0.2 mm for both beams.

The distance between the last pre-sample and first post-sample slits was 27 cm.

TiB$_2$ has an hexagonal structure with space group $P6/mmm$ - D_{6h}^1. At most pressures 8 peaks were used to determine the change in the lattice parameters a and c. Either directly as from the 100, 110, 200 reflections for a and the 001, 002 reflections for c, or by solving simultaneous equations for pairs of the other reflections. For an hexagonal unit cell the relevant equations are

$$\frac{1}{d^2} = \frac{4}{3a^2}\left(h^2 + hl + k^2\right) + \frac{l^2}{c^2}.$$

for the d-spacing with Miller indices hkl, and

$$V = a^2 c \sin(120^\circ).$$

for the volume of the unit cell.

The first five reflections of the copper spectrum were used to determine the pressures up to 130 $kbar$. The accuracy achieved in the pressure calibration, approximately 0.5%, is certainly as good or better than that reported in the literature to date. **Table 3** below contains the results of our measurements which are illustrated in **Figure 19 (a), (b)** and **(c)**.

Table 3 - Measured compressibility data of TiB$_2$ up to 130 kbar.

P(kbar)	±	a/a_o	c/c_o	V/V_o	
11.6	0.3	0.9987	0.9989	0.9963	0.0011
25.2	0.3	0.9985	0.9976	0.9946	0.0007
47.2	0.3	0.9968	0.9957	0.9893	0.0010
71.1	0.4	0.9961	0.9947	0.9869	0.0017
84.0	0.4	0.9930	0.9917	0.9778	0.0014
98.8	0.5	0.9944	0.9922	0.9811	0.0013
116.3	0.5	0.9927	0.9909	0.9764	0.0017
123.5	0.5	0.9913	0.9887	0.9716	0.0021
130.4	0.4	0.9886	0.9875	0.9651	0.0011
130.5	0.5	0.9884	0.9875	0.9648	0.0011
a_o=3.0274	±0.0008 (Å)	c_o=3.2282	±0.0009 (Å)	V_o=25.623	±0.012 (Å^3)

Figure 19 - Reduced lattice parameters and volume as a function of pressure for TiB_2. The straight lines are the results of least squares fits and the error bars represent standard deviations. The data plotted are: (a). a/a_o; (b). c/c_o; (c). V/V_o.
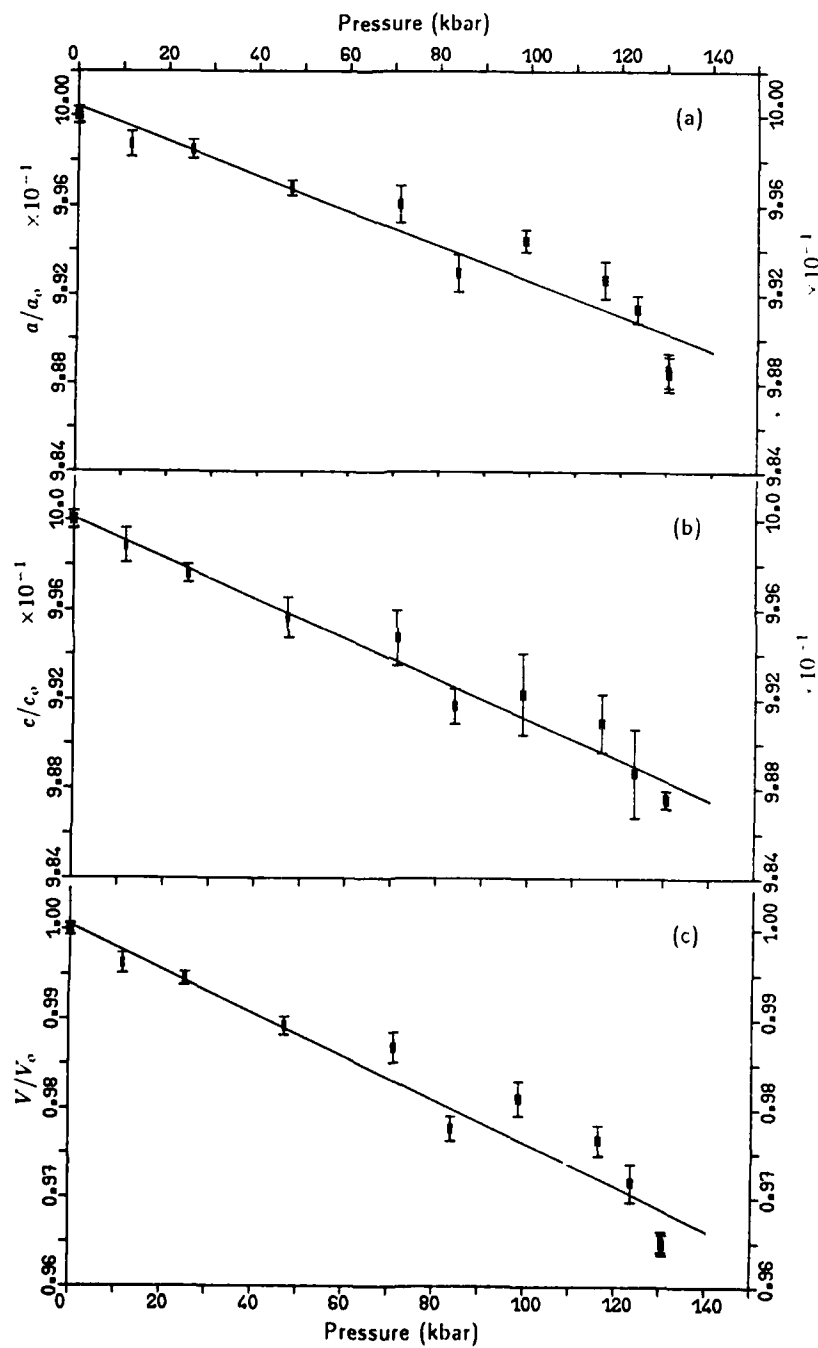
With a volume change of ~ 3% at 120 *kbar* (Figure 19(c)), TiB$_2$ is nearly as incompressible as diamond which has a bulk modulus K_o of 4.42 Mbar. That of TiB$_2$ was determined from the slope of the linear least squares fit to the V/V_o versus pressure data using the method described in Section 5.2.2. Its value was calculated as

$$K_o = 4.1 \pm 0.25 \; Mbar \;.$$

This value may be regarded as an upper limit as a least squares fit of a non-linear EOS would probably have yielded a slightly lower value. However, with such an incompressible material, and considering the scatter of the data obtained so far, we would require more points over a larger range of pressures to obtain a meaningful quadratic term. In any case, a new and improved value of K_o would most certainly be within the 6% standard deviation given above.

6 - Summary and Conclusion

We have combined the wide and smooth spectrum of white radiation produced by a high voltage generator with energy dispersive diffraction and a Drickamer-type high pressure cell and exploited the advantages of this new technique in high pressure measurements on TiB. High energy X-rays and energy dispersive diffraction produce:

(1) highly penetrating radiation;

(2) a wide range of energies;

(3) a high sensitivity to lattice parameter changes

The first feature is required to traverse the thick disc of packing surrounding the sample. The second feature is indispensable to resolve the reflections from the sample, pressure calibrant and packing. The third feature greatly improves the accuracy of the compressibility measurements.

TiB is far from an ideal material to study using EDXRD and to use for testing the high pressure technique developed here. It is a poor scatterer of X-rays with an orthorhombic structure and EDXRD is intrinsically a low resolution technique. Further, its low compressibility causes small changes in its lattice parameters with pressure and thus

lowers the accuracy of the measurements. Nevertheless, the simple experimental technique developed here has produced a reliable value of the bulk modulus of TiB, accurate to a few percent, from measurements of its compressibility over the pressure range of 0 to 80 $kbar$.

We have demonstrated that EDXRD can be combined with the high energy synchrotron radiation produced by the SRS $Wiggler$ to give an accuracy of a few parts in 10^4 in d-spacing measurements on such low symmetry materials.

We have also successfully combined the wide dynamic range of penetrating radiation produced by the $Wiggler$ with the Drickamer-type cell for high pressure studies of TiB_2. The brightness of the source and the high collimation of the radiation have enabled us to work with a geometry guaranteeing a high signal-to-noise-ratio and spectra free of contamination from the packing and anvils. With a relative accuracy of $2 \cdot 10^{-4}$ in measurements of changes in d-spacing, we have obtained state-of-the-art accuracy in compressibility measurements up to 130 $kbar$.

The technique developed here also promises good results in intensity measurements. Absolute measurements have not been attempted so far as the beam geometry was not optimised during the first visits to the SRS, but relative intensities have shown variations of only a few percent over the range 0 to 130 $kbar$. These indicate that little or no preferred orientation was introduced in the samples, and hence the existence of a nearly hydrostatic pressure distribution.

7 - Future Work

Further work is currently in progress on all the topics discussed in this report

An EDXRD setup is being built here in King's College. The present source of X-rays is a conventional 50 kV generator, but the purchase of a high voltage generator is being considered. Such a generator would enable us to reproduce the system which we have been using in Manchester with the added advantages of constant availability and more efficient use of our on-site ressources. Our setup will be used predominently to study the behaviour of our existing high pressure cells and compare the compressibilities of various potential pressure calibrants. The results of this work will lead to improvements in cell design and performance and the establishment of new secondary pressure calibrants.

Extensive use of the SRS Wiggler is also planned for further high pressure studies. We are currently involved in the design of a new experimental station dedicated to EDXRD and are collaborating with other research groups to plan the high pressure side of the experimental program. Several types of high pressure cells, including diamond anvil cells capable of reaching 500 *kbar* , will soon be available to us. At first we plan to concentrate our studies on pure titanium, titanium alloys and new titanium compounds. Measurements on TiB and TiB_2 will also be made at higher pressures than those reached so far. Later we will include other industrially and commercially interesting materials, and hence there is much scope for measurements and studies on any new materials available from the US Army Research Agencies.

In parallel with our high pressure work, we have also developed the technique for lattice parameter measurements. Energy dispersive diffraction and highly penetrating radiation allow measurements to be made from thick samples using a simple transmission geometry. This technique has a present accuracy of a few parts in 10^4, but the potential of reaching 1 part in 10^4. Further, as the generator is transportable and the technique is easy to use, it is suitable for experiments in the field as well as in the laboratory. Our current program of studies concentrates on the measurement of residual stress in absorbing materials for the US Army Material Technology Laboratories in Watertown (Contract DAJA45-86-M-0507).

8 - Contributions to Conferences and Meetings

The technique developed for the work presented in this report was the subject of a *poster* presented at the Annual Meeting of the British Crystallographic Association held at the University of York, England, in April 1986.

The results of the study on TiB were presented as a *poster* at the 24th Annual Meeting of the European High Pressure Research Group held at the University of Surrey, Guildford, England, in July 1986.

The work carried out on TiB_2 using synchrotron radiation and the Drickamer-type high pressure cell was the subject of a paper also presented at this meeting, but as an *oral contribution*.

The results obtained during the latest high pressure measurements on Ti, TiB and TiB$_2$ using synchrotron radiation will be presented as a *contributed paper* at the XIth AIRAPT International High Pressure Conference in Kiev. USSR. in July 1987. The paper will be published in the Conference Proceedings and will probably be an oral contribution.

Further independent publication of some of the results presented in this report as well as recent results obtained with synchrotron radiation is also planned.

9 - References

All the relevant references to the background work are given in D. Häusermann's Ph.D. thesis (see note on page 2) which describes in greater detail most of the material reported here. Two copies of this thesis are included with the copies of this report.

END

DATE
FILMED

4 - 87